Crustal strength in central Tibet determined from Holocene shoreline deflection around Siling Co

Citation	Shi, X., Kirby, E., Furlong, K. P., Meng, K., Robinson, R., & Wang, E. (2015). Crustal strength in central Tibet determined from Holocene shoreline deflection around Siling Co. Earth and Planetary Science Letters, 423, 145-154. doi:10.1016/j.epsl.2015.05.002
DOI	10.1016/j.epsl.2015.05.002
Publisher	Elsevier
Version	Accepted Manuscript
Terms of Use	http://cdss.library.oregonstate.edu/sa-termsofuse

Crustal strength in central Tibet determined from Holocene shoreline deflection around Siling Co

Xuhua Shi[a, b,*], Eric Kirby[c], Kevin P. Furlong[a], Kai Meng[d], Ruth Robinson[e], Erchie Wang[d]

[a] Department of Geosciences, Pennsylvania State University, University Park, PA 16802, USA

[b] Now at Earth Observatory of Singapore, Nanyang Technological University, Singapore 639798

[c] College of Earth, Ocean, and Atmospheric Sciences, Oregon State University, Corvallis, OR, USA

[d] Institute of Geology and Geophysics, Chinese Academy of Sciences, Beijing 100029, China

[e] Department of Earth and Environmental Sciences, University St Andrews, St Andrews KY16 9AL, Scotland, UK

* Corresponding author. E-mail: xshi@ntu.edu.sg

Abstract: Controversial end member models for the growth and evolution of the Tibetan Plateau demand quantitative constraints of the lithospheric rheology. Direct determinations of bulk crustal rheology, however, remain relatively sparse. Here we use the flexural rebound of lacustrine shorelines developed during the Lingtong highstand around Siling Co, in central Tibet, to place bounds on the effective elastic thickness (T_e) and viscosity of Tibetan crust. Shoreline features associated with the Lingtong highstand complex ~ 60 meters above present lake level are deflected from horizontal by 2-4 meters over wavelengths of ~ 200 kilometers. Optically stimulated luminescence dating of aggradational shoreline deposits indicate that these lake levels were reached at 6-4 ka. Assuming that surface loads were entirely supported by an elastic layer overlying an inviscid fluid, the range and spatial distribution of variations in shoreline elevation are consistent with deflections predicted by a uniform elastic plate with thickness, T_e of 20-30 km. If viscoelastic relaxation in response to lake withdrawal is complete, our data suggest an average viscosity $\leq 10^{19}$ Pa s. These results imply that the apparent viscosity of the lower crust inferred over millennial timescales is comparable with that estimated from post-seismic relaxation over decadal timescale.

Keywords: Crustal strength, Tibetan Plateau, lake shoreline, effective elastic thickness, viscosity

Highlights

- Shoreline deflection provides constraints on the strength of crust in central Tibet.
- A Mid-Late Holocene highstand shoreline around Siling Co is deflected by ~ 2-4 m.
- Shoreline deflections suggest an effective elastic thickness of ~ 20-30 km.
- If rebound is complete, crustal viscosity beneath Siling Co is $\leq (1\text{-}2) \times 10^{19}$ Pa s.

1. Introduction

The rheology of the deep crust in orogenic systems has long been understood to influence the distribution, rates and style of lithospheric deformation (Argand, 1924; England and Houseman, 1986; Zhao and Morgan, 1987). However, determining the rheologic properties of actively deforming lithosphere is difficult, and much of our understanding of the bulk rheology of continental crust relies on either laboratory estimates of the constitutive behavior of rock materials (Brace and Kohlstedt, 1980) or on measurements of transient surface deformation following large earthquakes (Bürgmann and Dresen, 2008; Savage and Prescott, 1978). To a large degree, debates over the distribution of strength in continental lithosphere (Jackson, 2002; Watts and Burov, 2003) and the related question of whether deformation is continuous between crust and mantle (England and Houseman, 1986), owe their persistence to the difficulty of knowing the rheologic properties of the lithosphere in space and time.

Few doubt that the middle and lower portions of the crust of the Tibetan Plateau have undergone deformation during the Indo-Asian collision, but the nature of this deformation is one of the more contentious questions in continental dynamics today. On one hand, it is argued that the plateau owes its very existence to widespread lateral flow of the deep crust (Bird, 1991; Royden et al., 1997; Royden et al., 2008; Shen et al., 2001). Abundant geophysical data indicate that the lower crust should be quite weak at high temperatures and in the presence of fluids (Bai et al., 2010; Brown et al., 1996; Fan and Lay, 2003; Klemperer, 2006; Makovsky and Klemperer, 1999; Nelson et al., 1996; Unsworth et al., 2005; Wei et al., 2001). Geologic observations from eastern Tibet implicate the large-scale influx of lower crust to explain the growth of plateau topography in that region (Royden et al., 2008), and, numerous aspects of the tectonic evolution of the Himalaya can be explained by channelized flow of crustal rocks from beneath Tibet

(Beaumont et al., 2001). On the other hand, however, the correspondence of geodetic velocity fields and the inferred directions of seismic anisotropy in the mantle supports the idea of vertically-coherent deformation throughout Tibetan lithosphere (Bendick and Flesch, 2007; Davis et al., 1997; Flesch et al., 2005; Holt, 2000; León Soto et al., 2012). Geological observations from xenoliths beneath Tibet suggest that portions of the lower crust may be fluid-poor (Hacker et al., 2000), and several key aspects of the geology of the Himalaya (Harrison, 2006) do not seem to require channel flow. Thus, the conflicting nature of these geophysical observations highlights the need for experiments to directly determine crustal rheology.

Here we approach this question of crustal flow by measuring surface deformation around a large lake, Siling Co (‘co’ or ‘tso’ are alternative English translations of the Tibetan word for lake) (Fig. 1), in central Tibet, that occurred in response to climatically induced changes in lake levels. Changes in the volume of lake systems represent a surface load on the lithosphere, and the consequent flexural response is sensitive to the flexural rigidity of the elastic portion of the crust, to the viscosity of the deep crust and/or mantle, and to the timescale of loading or unloading. Moreover, shorelines developed during highstand levels represent a paleo-horizontal datum from which to measure deflections, as well as provide an estimate of the volume of the load. This methodology is a proven means of estimating the bulk constitutive behavior of the lithosphere and has provided key constraints in the Basin and Range (Bills et al., 1994a; Gilbert, 1890), the Andes (Bills et al., 1994b), and in the Mediterranean (Govers et al., 2009). It has also been recently used to place bounds on the rheology of the crust in west-central Tibet (England et al., 2013). Central to these efforts is the notion that variations in water loads typically occur over timescales of several thousand years and across spatial scales of tens to hundreds of kilometers. The resultant estimates of lithospheric rheology thus can fill a gap between inferences derived from the geologic evolution of orogens over millions of years (Clark and Royden, 2000) and those derived from decadal measurements of surface deformation associated with the earthquake cycle (Hilley et al., 2005; Huang et al., 2014; Yamasaki and Houseman, 2012).

In this paper, we evaluate shoreline deformation around Siling Co in the central portion of the Tibetan Plateau. This lake resided at ~ 4530 m in 1976 and extended over an area of ~ 1660 km^2 (Meng et al., 2012a), but water levels have been increasing in elevation (by ~12 m) and area over the past several decades (Meng et al., 2012a). The lake is situated just south of the Banggong-Nujiang suture (Fig. 1) separating the Lhasa and Qiangtang terranes, and lies just to the west of the primary profile of the INDEPTH 3 geophysical experiment (Ross et al., 2004; Zhao et al., 2001). Flights of Late Pleistocene-Holocene shorelines are preserved at elevations up to ~ 100 m above present lake level (Li et al., 2009). We combine geomorphic mapping and surveying of shoreline elevations (Meng et al., 2012b) with new optically stimulated luminescence (OSL) ages to develop the chronology of shoreline features that allows us to constrain the amplitude, wavelength and timescale of shoreline rebound and deformation. We utilize these data in a 3D single-layered elastic model to evaluate the effective elastic thickness (a proxy for flexural rigidity or elastic strength) of the Tibetan crust beneath Siling Co. Finally, we use the timescale of the shoreline rebound to estimate the viscosity of the lower crust by assuming a viscous support of the water load.

2. Geomorphology, deflection and age of shorelines around Siling Co

2.1 Shoreline geomorphology

Extensive flights of relict shorelines are preserved around Siling Co and its neighboring lakes. Mapping these shorelines using high resolution (0.5 m nominal resolution) satellite imagery (Fig. 2) reveals a prominent group of shoreline features at ~ 4594 m elevation that mark a continuous and distinct boundary between older geomorphic features above the shoreline level and younger features below. The shoreline is characterized by constructional features such as beach ridges, spits, tombolos and cuspate bars and erosional wave-cut scarps that cut across both alluvial fans and bedrock (Fig. 2). The landscape above the highstand shoreline exhibits geomorphic characteristics that are consistent with significant age; alluvial fans truncated by wave-cut scarps along this shoreline complex are dissected by deep gullies and channels. Relict, discontinuous shoreline features are found above ~ 4594 m (Li et al., 2009), but these tend to be degraded and poorly preserved. Some exhibit polygonal "patterned ground" consistent with a protracted period of permafrost activity (Jorgenson et al., 2006). In contrast, the landscape below the shoreline complex at ~4594 m is characterized by groups of laterally continuous beach ridges developed across a strandplain. Beach ridges are fresh, undissected, and only the most active alluvial fans drape them (Fig. 2). Thus, the shoreline complex at ~ 4594 m elevation appears to represent a highstand strandline that was extensive around Siling Co; recession from this level was marked by the deposition of multiple beach ridges, possibly reflecting short-lived stillstands. The wide spatial distribution and continuity of the highstand shoreline on both central peninsulas and along the margins of Siling Co makes this an ideal marker from which to measure variations in shoreline deflection with location. For convenience, we name this highstand shoreline at ~ 4594 m as the '*Lingtong*' shoreline, after the name of a nearby village at the southeastern margin of this lake where the shoreline is well exposed.

2.2 Shoreline deflections

To determine current relative elevations along the Lingtong shoreline, we focused on the elevations of constructional features. These have several advantages over wave-cut cliffs/scarps in determining the position of the ancient lake level (Adams and Wesnousky, 1998): 1) the elevation of swash surfaces along the shoreface represents a reasonable estimate of mean water level during formation of the beach barrier; 2) well-preserved flat crests of constructional shorelines are relatively easy to survey; and 3) the sediments that comprise constructional features afford the potential for determining the timing of shoreline development. Wave-cut cliffs retreat during successive undercutting and failure, and burial of the shoreline angle at the base of wave-cut scarps during scarp retreat can make determining precise elevations difficult.

We surveyed constructional features at 66 localities along the Lingtong highstand shoreline using differential GPS (Meng et al., 2012a) that allowed us to measure relative differences in ellipsoidal elevation with precision at the decimeter level (see Supplemental Materials). Shoreline features associated with longshore transport (spits and tombolos) were surveyed at the point of attachment to the shoreline. These positions likely represent a minimum estimate of water elevation at time of the shoreline occupation. Beach ridges and cuspate bars are considered more reliable, as they likely formed at, or immediately above, the fair weather wave base (Tanner, 1995). Measurement uncertainties on any given survey site are small and reflect effects of positioning and baseline processing (~ 0.1 m, Meng et al., 2012a). Moreover, the relatively smooth topography along shoreline surfaces exhibits limited variations in elevation (typically < 20-50 cm), and thus we consider that they represent a reasonable estimate of lake level to within ~1 m.

We also assign a nominal quality rank to each feature that represents the likelihood that each of our surveyed shoreline features represents occupation of a once continuous lake level (Fig. 3). Sites in which we have the highest confidence (rank A) have clear association with the geomorphic boundary between relict alluvial deposits and lacustrine deposits. Typically, these are depositional features that can be traced continuously into wave-cut scarps, and mark the highest occupation of the former lake. We also assign shoreline to this group that have independent age control (see below). Lower confidence (rank B) is placed in sites that express very sharp and prominent depositional morphology, but cannot be traced continuously into the highest shoreline level. These shoreline features may be developed during occupation of the Lingtong complex, but may not have developed during occupation of the highest position. Our lowest confidence sites (rank C) exhibit neither sharp features nor clear continuity or connection with the sharp geomorphic boundary; in some places the shorelines are ambiguous with respect to the Lingtong highstand level. Together, rank A and B sites constitute ~86% of the full data set (Table S4 in Supplemental Material and supplemental Google Earth kmz file).

Our results reveal limited variation in relative heights of the surveyed shoreline features at the Lingtong highstand level, along a radial distance up to 110 km away from the centroid of the water load (Fig. 3B and Fig. 4A). Fifty-eight out of sixty-six (87.8%) shorelines reside at elevations between 4593 m and 4595 m, within 1 m of the mean elevation (4593.9 m). Notably, nearly all shorelines with confidence level A lie within this 2 m range (Fig. 3B and Fig. 4A). Shorelines of confidence levels B and C exhibit a larger range of elevation, up to ~4.5 m; most of these lie near the center of the load (Fig. 3B). The vertical elevation ranges at a specific radial distance (Fig. 3, B and C) may reflect both 1) the complicated deflection pattern due to the complex load geometry (Fig. 4, B and C), and 2) variations in the shoreline surface heights relative to the mean water level associated with site-specific variations in local wave energy, basal topography, sediment supply and duration of activity for shorelines during the shoreline development (Adams and Wesnousky, 1998; Bills et al., 2007; Gilbert, 1890). Thus we consider that the full range of variation (~4.5 meters) a maximum allowable bound on the magnitude of deflection. We conclude that the deflection range of the Lingtong highstand shorelines is most likely 2 m, and possibly up to 4 m.

It is noteworthy that shorelines east of the lake center appear to decrease systematically, by ~1.5-2 meters, toward the east (Fig. 3C). Similarly, shorelines around Wuru Co, west of the centroid of water mass, appear to also decrease from west to east by ~1.5-2 meters (Fig. 3C). Although we cannot rule out that these variations are coincidental, given uncertainties, it is possible that Lingtong highstand shorelines record a long-wavelength, regional tilt.

2.3 Shoreline ages

The timing of deposition of shoreline deposits supports the correlation of highstand shorelines and constrains the timing and duration of lake loads. Age control of the shorelines around Siling Co is limited; existing OSL dates from beach deposits range from ~ 70 ka to as young as ~ 6 ka (Li et al., 2009) and generally suggest lake recession since 70 ka. Exposure age dating of bedrock outcrops interpreted to be wave-cut platforms, however, yield ages as old as ~160 ka to ~ 250 ka (Kong et al., 2011), suggesting the possibility of an older and more complicated history. In contrast, the highstand shorelines around Gyaring Co, which is ~ 70 km southwest of Siling Co but within the upstream Siling Co drainage basin, show OSL ages of 4-5 ka (Shi et al., 2014). These debates highlight the need to better constrain the ages of highstand shorelines in central Tibet.

In this study, we collected 9 samples of medium- and fine-grained sand and silt layers intercalated within beach gravels for OSL dating of the age of the Lingtong highstand shoreline complex from 9 sites around the lake (Fig. 3A). Analysis and interpretation of luminescence data are described in Supplemental Material. Our results reveal that 7 of the 9 samples yield ages that cluster between ~ 4-6 ka (Table 1); two of these samples come from shorelines near the center of the lake (OSL sample numbers 6 and 34 in Fig. 3A) and five samples represent positions along the southeastern and western margin of the lake (OSL-1, 25, 31, 33, 46 in Fig. 3A), confirming our interpretation that the shoreline complex represents features developed during a single highstand. Two samples (OSL-21 and OSL-32) have ages that deviate from this cluster of results. These samples have large overdispersion of individual aliquots and appear to contain multiple components in the distribution of De (see Supplemental Material). OSL-21 has an age of ~ 3.9 ka based on the younger De component of 3 aliquots using a finite mixture model (see Supplemental Material), which is consistent with the age range of 4-6 ka for other samples (Table 1; Fig. S2D). However, the older component of the distribution suggests an age of ~7.8 ka. If this component is a reliable burial age, it might suggest that the duration of shoreline development occurred during 8-4 ka. The other sample, OSL-32 from a shoreline of quality rank C in the shoreline correlation, has an age of 1.5 ka calculated by minimum age model-3 (see Supplemental Material), significantly younger than the other samples. We also observed evidence for bioturbation by rodents at this locality (although not directly in our sample location), and it is possible that this sample may have been influenced by bioturbation. Collectively, the OSL chronology from shoreline complex suggest features were developed during a highstand that occurred from 6-4 ka. Importantly, our results place constraints on the timing of initial recession of the lake (ca. 4 ka), which provides a bound on the timescale of shoreline deflection.

3. Rigidity of Tibetan crust from flexural rebound

We determine the flexural rigidity (D) of Tibetan crust through analysis the effective elastic thickness (T_e). The relationship between the two parameters is described as

$$D \equiv \frac{ET_e^3}{12(1-\nu^2)}, (1)$$

where E is Young's modulus and ν is Poisson's ratio. We estimate T_e by comparing our observed shoreline elevation data with the predicted deflection of an infinite elastic slab overlying an inviscid substrate in response to a spatially varying load that represents the change in lake level. Implicit in this analysis is the assumption that measured shoreline deflection represents the full response to the lake withdrawal. We represent the load as an irregular volume consistent with the height and geometry of the Lingtong highstand shorelines above present lake level (see Fig. 4, B and C). We assume a uniform T_e of the crust beneath Siling Co. We calculate the crustal flexural response (hence the pattern of shoreline deflection) to lake unloading over a range of flexural rigidities that reflect T_e variations from 2 km to 50 km (see examples in Fig. 5, A-C and Fig. 6). We adopt the analytical solutions to the pseudo-3D equation of flexure of a thin elastic spherical shell under a disc-shaped load (Brotchie and Silvester, 1969; Watts, 2001, and see details in Supplemental Material). The computation scheme follows the method of Nakiboglu and Lambeck (1983). In the scheme, the water load has been discretized to cylinders with diameter of 1 km and varying heights, and the total flexure of the lithosphere is calculated by sum of the flexure in response to loading of each unit cylinder (see Supplemental Material).

We search for best estimates of T_e using two criteria. First, we seek a condition where the maximum difference in predicted deflection equals the range of shoreline deflections (~ 2 m, and perhaps 4 m, as discussed above). Second, we calculate a root mean square (RMS) of the misfit between the calculated (Fig. 5, A-C and Fig. 6) and observed deflections. Because the elevation datum of 'zero' deflection is not known *a priori,* observed deflections are represented by the deviations of the shoreline elevations from their mean (Fig. 4A). We recognize that this approach is limited; shorelines are not preserved in a spatially uniform distribution, and thus the RMS may be weighted to regions with more data. Nonetheless, it serves as a useful complement to the predicted range in shoreline deflection.

Comparison of the results of forward models with varying elastic thickness (Fig. 5 and Fig. 6) show that deflections are best fit with a T_e of ~30 km. At this elastic thickness, the calculated deflection range is nearly equal to the vertical elevation range of ~ 2 m (Fig. 5E), among all Lingtong highstand shorelines of high confidence (ranks A and B). If we consider the possibility that deflections range up to 4 m, an elastic thickness of ~20 km is allowable. Differences in RMS of the misfit for these models is small, ranging from 0.86 to 1.22 (Fig. 6). Although the RMS measure of misfit continues to decrease slightly for larger T_e of 40 km (Fig. 6), range of predicted deflections underpredicts the observed deflection of 2-4 m. Thus, we conclude that the observed deflections of the Lingtong highstand shorelines implies an elastic lithosphere of T_e ~ 20-30 km around Siling Co in central Tibet.

One important caveat is that this estimate of T_e assumes complete rebound of the Lingtong shoreline. If the rebound is incomplete, perhaps due to ongoing viscoelastic rebound (see next section), the observed deflections of 2-4 m represent only a fraction of the total. In this case, the "true" T_e would be somewhat lower than 20-30 km (Willett et al., 1985). Unfortunately, we are not able to test this assumption with our current data; deflection of a lower set of shorelines around Siling Co could be used to determine the degree of recovery, similar to studies in the Lake Bonneville basin in the western United States (Passey, 1981). However, given that deflection of a lower set of shorelines, if any, is expected to be smaller than that of the Lingtong highstand, the uncertainties associated with determining lake levels from preserved shoreline features would prevent determination of deflection.

4. Viscosity of central Tibetan crust

An alternative interpretation assumes that viscous stresses arising from flow of crust beneath the elastic upper layer support surface loading (England et al., 2013). Given that the elastic thickness implied by our results is significant less than the crustal thickness in central Tibet (~65 $\pm$5 km) (Nábělek et al., 2009; Zhao et al., 2001), this is a reasonable possibility. If we assume that the observed flexural rebound of the elastic layer represents complete adjustment by viscous flow in the lower crust, the timescale of the lake unloading places a maximum bound on crustal viscosity of central Tibet. The viscosity that would allow complete compensation of the removal of the lake load in the available time can be simply approximated by

$$\eta = \frac{\rho g \lambda}{4\pi}\tau_r \qquad (2),$$

where τ_r is the characteristic e-folding relaxation time that is approximately 1/3 of the total relaxation time (τ_T) (Turcotte and Schubert, 2002). Here τ_T is assumed to be ~ 4 ka, the minimum age of recession from the Lingtong highstand level; η is the viscosity of the compensating medium; ρ is the density of the compensating fluid (here assumed to be 2900 kg/m^3); g is gravitational acceleration (9.8 m/s^2); and λ is the flexural wavelength (~ 150-200 km) estimated from the flexural wavelength of the load. This simple analysis implies that, in order for complete relaxation of the crust in response to removal of the load, the average viscosity of the lower crust beneath Siling Co would have to be $\leq$ (1-2)$\times 10^{19}$ Pa s. However, the assumption of complete adjustment makes this value less certain; if viscoelastic relaxation is still ongoing, the effective viscosity would be greater (Willett et al., 1985). One consideration in both of these estimates, however, is that the loading phase of the lake may have been relatively short; our chronology strictly imply a duration of ~2 ka (6 to 4 ka), and we do not have independent data that constrain when the lake reached its highstand level.

5. Discussion

5.1 Elastic strength of central Tibetan crust

Our study contributes to an emerging body of constraints on the effective elastic structure of Tibetan crust over millennial timescales. The elastic thickness of 20-30 km determined in this study is less than half of the crustal thickness in central Tibet, which is 65 ± 5 km (Nábělek et al., 2009; Zhao et al., 2001). Since the elastic thickness reflects a depth integration of the crustal strength (Watts, 2001), our results argues that central Tibetan crust may be relatively weak, generally consistent with the observation that focal depths of large earthquakes in Tibet are largely confined to the upper ~15-20 km of the crust (Chu et al., 2009).

Values for T_e of 20-30 km in Siling Co region from millennial lake loading history are comparable with T_e estimates for the same area from plateau-scale gravity anomalies and topography, considering the uncertainties in the estimates and the relatively low resolution of gravity and topographic data. These estimates are T_e ~ 20-30 km (Braitenberg et al., 2003; Jordan and Watts, 2005) or 20-40 km (Audet and Bürgmann, 2011; Chen et al., 2015). But our T_e estimates of Siling Co region are higher than those (mostly T_e < 20 km) in neighboring regions and much of central and northern Tibet (Braitenberg et al., 2003; Chen et al., 2015; Jordan and Watts, 2005; Masek et al., 1994). Regional variation in these estimates may reflect heterogeneity of crustal strength, potentially associated with difference in inherited localized thermal regimes (Harrison, 2006; Hetényi et al., 2011).

5.2 Consistent viscosity of central Tibetan lower crust on decadal and millennial timescale

The bound on the average viscosity of the crust in central Tibet of ~ (1-2) $\times 10^{19}$ Pa s determined in this study is consistent to the results of a similar study of shorelines around Zhari Nam Co in west-central Tibet (Fig. 1) (England et al., 2013). Here, the apparent absence of shoreline deflection also argues for a crustal viscosity > 10^{19}-10^{20} Pa s (England et al., 2013). Notably, our dating of shoreline occupation at Siling Co is also consistent with the lake loading histories assumed by England et al. (2013) and lends support to the notion that lake level changes were synchronous across much of the interior of the Tibetan Plateau during Holocene time.

These viscosity estimates of lower crust from shoreline rebound are also generally consistent with estimates developed from models of transient deformation following earthquakes (Fig. 7 and Table S5). In 2008, the M_w 6.4 Nima-Gaize earthquake occurred along a small graben approximately 300 km to the west of Siling Co (Fig. 1); viscoelastic models place a lower bound on the viscosity of a Maxwell half-space of ~3 $\times 10^{17}$ Pa s (Ryder et al., 2010) (Fi.g 7). Similarly, the lack of resolvable post-seismic deformation after the 2008 M_w 6.3 normal faulting event at Damxung, along the central portion of the Yadong-Gulu rift, approximately 250 km to the southeast of Siling Co (Fig. 1), suggests a lower bound of ~1 $\times 10^{18}$ Pa s for crustal viscosity (Bie et al., 2014). Finally, decadal measurements (1992–2010) of surface deformation following the 1951 and 1952 earthquakes in the Ben Co region, ~ 200 km east of Siling Co (Fig. 1), constrain lower crustal viscosities to (5-10) $\times 10^{19}$ Pa s (Ryder et al., 2014). Although the lower bounds of these data imply somewhat lower viscosities than our study (Figure 7), the overlap between decadal and millennial timescale observations suggest that the lower crust beneath central Tibet is likely on the order of 10^{19} Pa s.

A synthesis of data from other parts of the Tibetan plateau (Fig. 7), suggests that the viscosity of the crust likely varies across the orogen. Transient deformation along the Kunlun fault system following the 1997 M_w 7.6 Manyi and the 2001 M_w 7.9 Kokoxilli earthquakes implies lower crustal viscosities > 10^{18} Pa s (Hilley et al., 2005; Hilley et al., 2009) and perhaps in the range of $(1\text{-}5)\times10^{19}$ Pa s (Ryder et al., 2011; Wen et al., 2012). In eastern Tibet, adjacent to the Sichuan basin, however, transient deformation following the 2008 Wenchuan M_w 7.9 event implies a relatively weak lower crust (Shao et al., 2011), with viscosities on the order of 10^{18} Pa s (Huang et al., 2014). These regional differences appear to imply relatively large spatial changes in ductile strength of the lower crust in Tibet.

5.3 Implications for lower crustal flow

Numerous efforts to explain the present-day topography of the plateau argue for a weak lower/middle crust (Bendick et al., 2008; Clark et al., 2005; Clark and Royden, 2000; Cook and Royden, 2008; Copley and McKenzie, 2007; Royden et al., 1997); models of the geologic evolution of the plateau invoke effective viscosities ranging from 10^{16}-10^{22} Pa s (also see Table S6 in Supplemental Material). Thermal-mechanical numerical models parameterized to mimic constitutive flow laws (Beaumont et al., 2001) imply that extensive flow in a lower crustal channel may develop once the effective viscosity reaches values of ~ 10^{19} Pa s (Beaumont et al., 2004; Medvedev and Beaumont, 2006). Tradeoffs between the viscosity and the thickness of flow in a crustal channel make this value approximate (Bendick et al., 2008; Klemperer, 2006). In our study, as with that of England et al. (2013), the lower bound on crustal viscosity required by shoreline rebound is similar to this value, $(1\text{-}2)\times10^{19}$ Pa s. Thus, although our data permit wholesale flow of lower crust on geological timescales (Bird, 1991; Nelson et al., 1996), they are not consistent with the presence of a weak middle crust capable of channelized flow.

6. Conclusions

Deflection of Holocene shorelines around Siling Co provides a quantitative estimate of the rheology of central Tibetan crust. Recession of Siling Co by ~ 60 m from the Lingtong highstand conditions during the past 4-6 ka resulted in ~2-4 m of shoreline deflection from horizontal. Forward modeling of rebound of an elastic plate overlying an inviscid fluid in response to a spatially distributed surface load constrains the T_e to ~20- 30 km. Assuming that viscoelastic relaxation of crust beneath the elastic lid is complete requires a maximum average viscosity of ~ (1-2)$\times 10^{19}$ Pa s. If viscoelastic rebound is still ongoing, however, the tradeoff between rigidity of the elastic lid and viscosity of the underlying fluid, these values reflect an upper bound on strength and a lower bound on viscosity (Willett et al., 1985). Nonetheless, our results are consistent with viscosities estimated from shoreline deformation elsewhere in central Tibet (England et al., 2013) as well as with decadal measurements of post-seismic surface deformation (e.g., Ryder et al., 2014). Collectively, these data suggest that the crust in central Tibet, while weak, is not sufficiently so as to enable channelized flow in the middle crust.

Acknowledgments

This work was supported by a National Science Foundation grant (EAR-0911587) to E.K. and K.P.F. Additional support to E.W. was provided by grants from the Chinese Academy of Sciences (XDB03010500). We thank Phillip England and Roland Bürgmann for providing critical comments that significantly improved the manuscript.

References

Adams, K.D., Wesnousky, S.G., 1998. Shoreline processes and the age of the Lake Lahontan highstand in the Jessup embayment, Nevada. Geological Society of America Bulletin 110, 1318-1332.

Argand, E., 1924. La tectonique de l'Asie, International Geological Congress, 13th, Proceedings, pp. 171-372.

Audet, P., Burgmann, R., 2011. Dominant role of tectonic inheritance in supercontinent cycles. Nature Geosci 4, 184-187.

Bai, D., Unsworth, M.J., Meju, M.A., Ma, X., Teng, J., Kong, X., Sun, Y., Sun, J., Wang, L., Jiang, C., Zhao, C., Xiao, P., Liu, M., 2010. Crustal deformation of the eastern Tibetan plateau revealed by magnetotelluric imaging. Nature Geosci 3, 358-362.

Beaumont, C., Jamieson, R.A., Nguyen, M.H., Lee, B., 2001. Himalayan tectonics explained by extrusion of a low-viscosity crustal channel coupled to focused surface denudation. Nature 414, 738-742.

Beaumont, C., Jamieson, R.A., Nguyen, M.H., Medvedev, S., 2004. Crustal channel flows: 1. Numerical models with applications to the tectonics of the Himalayan-Tibetan orogen. J. Geophys. Res. 109, B06406.

Bendick, R., Flesch, L., 2007. Reconciling lithospheric deformation and lower crustal flow beneath central Tibet. Geology 35, 895-898.

Bendick, R., McKenzie, D., Etienne, J., 2008. Topography associated with crustal flow in continental collisions, with application to Tibet. Geophysical Journal International 175, 375-385.

Bie, L., Ryder, I., Nippress, S.E.J., Bürgmann, R., 2014. Coseismic and post-seismic activity associated with the 2008 Mw 6.3 Damxung earthquake, Tibet, constrained by InSAR. Geophysical Journal International 196, 788-803.

Bills, B.G., Adams, K.D., Wesnousky, S.G., 2007. Viscosity structure of the crust and upper mantle in western Nevada from isostatic rebound patterns of the late Pleistocene Lake Lahontan high shoreline. Journal of geophysical research 112.

Bills, B.G., Currey, D.R., Marshall, G.A., 1994a. Viscosity estimates for the crust and upper mantle from patterns of lacustrine shoreline deformation in the Eastern Great Basin. J. Geophys. Res. 99, 22059-22086.

Bills, B.G., de Silva, S.L., Currey, D.R., Emenger, R.S., Lillquist, K.D., Donnellan, A., Worden, B., 1994b. Hydro-isostatic deflection and tectonic tilting in the central Andes: Initial results of a GPS survey of Lake Minchin shorelines. Geophys. Res. Lett. 21, 293-296.

Bird, P., 1991. Lateral Extrusion of Lower Crust From Under High Topography in the Isostatic Limit. J. Geophys. Res. 96, 10275-10286.

Brace, W.F., Kohlstedt, D.L., 1980. Limits on Lithospheric Stress Imposed by Laboratory Experiments. J. Geophys. Res. 85, 6248-6252.

Braitenberg, C., Wang, Y., Fang, J., Hsu, H.T., 2003. Spatial variations of flexure parameters over the Tibet-Quinghai plateau. Earth and Planetary Science Letters 205, 211-224.

Brotchie, J., Silvester, R., 1969. On crustal flexure. Journal of geophysical research 74, 5240-5252.

Brown, L.D., Zhao, W.J., Nelson, D.K., Hauck, M., Alsdorf, D., Ross, A., Cogan, M., Clark, M., Liu, X.W., Che, J.K., 1996. Bright spots, structure, and magmatism in southern Tibet from INDEPTH seismic reflection profiling. Science 274, 1688-1690.

Bürgmann, R., Dresen, G., 2008. Rheology of the Lower Crust and Upper Mantle: Evidence from Rock Mechanics, Geodesy, and Field Observations. Annual Review of Earth and Planetary Sciences 36, 531-567.

Chen, B., Liu, J., Chen, C., Du, J., Sun, Y., 2015. Elastic thickness of the Himalayan–Tibetan orogen estimated from the fan wavelet coherence method, and its implications for lithospheric structure. Earth and Planetary Science Letters 409, 1-14.

Chu, R., Zhu, L., Helmberger, D.V., 2009. Determination of earthquake focal depths and source time functions in central Asia using teleseismic P waveforms. Geophysical Research Letters 36.

Clark, M.K., Bush, J.W.M., Royden, L.H., 2005. Dynamic topography produced by lower crustal flow against rheological strength heterogeneities bordering the Tibetan Plateau. Geophysical Journal International 162, 575-590.

Clark, M.K., Royden, L.H., 2000. Topographic ooze: Building the eastern margin of Tibet by lower crustal flow. Geology 28, 703-706.

Cook, K.L., Royden, L.H., 2008. The role of crustal strength variations in shaping orogenic plateaus, with application to Tibet. Journal of Geophysical Research-Solid Earth 113, -.

Copley, A., McKenzie, D., 2007. Models of crustal flow in the India–Asia collision zone. Geophysical Journal International 169, 683-698.

Davis, P., P. England and G. Houseman (1997). "Comparison of shear wave splitting and finite strain from the India-Asia collision zone." Journal of Geophysical Research: Solid Earth 102(B12): 27511-27522.

DeVries, P.M.R., Meade, B.J., 2013. Earthquake cycle deformation in the Tibetan plateau with a weak mid-crustal layer. Journal of Geophysical Research: Solid Earth 118, 3101-3111.

Ekström, G., M. Nettles, and A. M. Dziewonski, The global CMT project 2004-2010: Centroid-moment tensors for 13,017 earthquakes, Phys. Earth Planet. Inter., 200-201, 1-9, 2012. doi:10.1016/j.pepi.2012.04.002

England, P., Houseman, G., 1986. Finite Strain Calculations of Continental Deformation 2. Comparison With the India-Asia Collision Zone. J. Geophys. Res. 91, 3664-3676.

England, P.C., Walker, R.T., Fu, B., Floyd, M.A., 2013. A bound on the viscosity of the Tibetan crust from the horizontality of palaeolake shorelines. Earth and Planetary Science Letters 375, 44-56.

Fan, G.-W., Lay, T., 2003. Strong Lg Attenuation in the Tibetan Plateau. Bulletin of the Seismological Society of America 93, 2264-2272.

Fielding, E.J., McKenzie, D., 2012. Lithospheric flexure in the Sichuan Basin and Longmen Shan at the eastern edge of Tibet. Geophysical Research Letters 39.

Flesch, L.M., Holt, W.E., Silver, P.G., Stephenson, M., Wang, C.-Y., Chan, W.W., 2005. Constraining the extent of crust–mantle coupling in central Asia using GPS, geologic, and shear wave splitting data. Earth and Planetary Science Letters 238, 248-268.

Gilbert, G., 1890. Lake Bonneville. United States Geological Survey.

Govers, R., Meijer, P., Krijgsman, W., 2009. Regional isostatic response to Messinian Salinity Crisis events. Tectonophysics 463, 109-129.

Hacker, B.R., Gnos, E., Ratschbacher, L., Grove, M., McWilliams, M., Sobolev, S.V., Wan, J., Wu, Z.H., 2000. Hot and dry deep crustal xenoliths from Tibet. Science 287, 2463-2466.

Harrison, T.M., 2006. Did the Himalayan Crystallines extrude partially molten from beneath the Tibetan Plateau? Geological Society, London, Special Publications 268, 237-254.

Hetényi, G., Vergne, J., Bollinger, L., Cattin, R., 2011. Discontinuous low-velocity zones in southern Tibet question the viability of the channel flow model. Geological Society, London, Special Publications 353, 99-108.

Hilley, G.E., Bürgmann, R., Zhang, P.Z., Molnar, P., 2005. Bayesian inference of plastosphere viscosities near the Kunlun Fault, northern Tibet. Geophys. Res. Lett. 32, L01302.

Hilley, G.E., Johnson, K.M., Wang, M., Shen, Z.K., Burgmann, R., 2009. Earthquake-cycle deformation and fault slip rates in northern Tibet. Geology 37, 31-34.

Holt, W. E. (2000). Correlated crust and mantle strain fields in Tibet. Geology 28(1): 67-70.

Huang, M.-H., Bürgmann, R., Freed, A.M., 2014. Probing the lithospheric rheology across the eastern margin of the Tibetan Plateau. Earth and Planetary Science Letters 396, 88-96.

Jackson, J., 2002. Strength of the continental lithosphere: Time to abandon the jelly sandwich? GSA Today 12, 4-9.

Jordan, T.A., Watts, A.B., 2005. Gravity anomalies, flexure and the elastic thickness structure of the India–Eurasia collisional system. Earth and Planetary Science Letters 236, 732-750.

Jorgenson, M.T., Shur, Y.L., Pullman, E.R., 2006. Abrupt increase in permafrost degradation in Arctic Alaska. Geophysical Research Letters 33, L02503.

Klemperer, S.L., 2006. Crustal flow in Tibet: geophysical evidence for the physical state of Tibetan lithosphere, and inferred patterns of active flow. Geological Society, London, Special Publications 268, 39-70.

Kong, P., Na, C., Brown, R., Fabel, D., Freeman, S., Xiao, W., Wang, Y., 2011. Cosmogenic 10Be and 26Al dating of paleolake shorelines in Tibet. Journal of Asian Earth Sciences 41, 263-273.

León Soto, G., Sandvol, E., Ni, J.F., Flesch, L., Hearn, T.M., Tilmann, F., Chen, J., Brown, L.D., 2012. Significant and vertically coherent seismic anisotropy beneath eastern Tibet. J. Geophys. Res. 117, B05308.

Li, D., Li, Y., Ma, B., Dong, G., Wang, L., Zhao, J., 2009. Lake-level fluctuations since the Last Glaciation in Selin Co (lake), Central Tibet, investigated using optically stimulated luminescence dating of beach ridges. Environmental Research Letters 4, 1-10.

Makovsky, Y., Klemperer, S.L., 1999. Measuring the seismic properties of Tibetan bright spots: Evidence for free aqueous fluids in the Tibetan middle crust. J. Geophys. Res. 104, 10795-10825.

Masek, J.G., Isacks, B.L., Fielding, E.J., Browaeys, J., 1994. Rift flank uplift in Tibet: Evidence for a viscous lower crust. Tectonics 13, 659-667.

Medvedev, S., Beaumont, C., 2006. Growth of continental plateaus by channel injection: models designed to address constraints and thermomechanical consistency. Geological Society, London, Special Publications 268, 147-164.

Meng, K., Shi, X., Wang, E., Liu, F., 2012a. High-altitude salt lake elevation changes and glacial ablation in Central Tibet, 2000–2010. Chinese Science Bulletin 57, 525-534.

Meng, K., Shi, X., Wang, E., Su, Z., 2012b. Geomorphic characteristics, spatial distribution of paleoshorelines around the Siling Co area, central Tibet, and the lake evolution within the plateau. Chinese Journal of Geology 47, 730-745 (in Chinese with English abstract).

Nábělek, J., Hetényi, G., Vergne, J., Sapkota, S., Kafle, B., Jiang, M., Su, H., Chen, J., Huang, B.-S., Team, t.H.-C., 2009. Underplating in the Himalaya-Tibet Collision Zone Revealed by the Hi-CLIMB Experiment. Science 325, 1371-1374.

Nakiboglu, S.M., Lambeck, K., 1983. A reevaluation of the isostatic rebound of Lake Bonneville. Journal of Geophysical Research 88, 10439-10410,10447.

Nelson, K.D., Zhao, W., Brown, L.D., Kuo, J., Che, J., Liu, X., Klemperer, S.L., Makovsky, Y., Meissner, R., Mechie, J., Kind, R., Wenzel, F., Ni, J., Nabelek, J., Leshou, C., Tan, H., Wei, W., Jones, A.G., Booker, J., Unsworth, M., Kidd, W.S.F., Hauck, M., Alsdorf, D., Ross, A., Cogan, M., Wu, C., Sandvol, E., Edwards, M., 1996. Partially Molten Middle Crust Beneath Southern Tibet: Synthesis of Project INDEPTH Results. Science 274, 1684-1688.

Passey, Q.R., 1981. Upper Mantle Viscosity Derived from the Difference in Rebound of the Provo and Bonneville Shorelines - Lake Bonneville Basin, Utah. Journal of Geophysical Research 86, 1701-1708.

Ross, A.R., Brown, L.D., Pananont, P., Nelson, K.D., Klemperer, S., Haines, S., Wenjin, Z., Jingru, G., 2004. Deep reflection surveying in central Tibet: lower-crustal layering and crustal flow. Geophysical Journal International 156, 115-128.

Royden, L.H., Burchfiel, B.C., King, R.W., Wang, E., Chen, Z.L., Shen, F., Liu, Y.P., 1997. Surface deformation and lower crustal flow in eastern Tibet. Science 276, 788-790.

Royden, L.H., Burchfiel, B.C., van der Hilst, R.D., 2008. The geological evolution of the Tibetan plateau. Science 321, 1054-1058.

Ryder, I., Bürgmann, R., Pollitz, F., 2011. Lower crustal relaxation beneath the Tibetan Plateau and Qaidam Basin following the 2001 Kokoxili earthquake. Geophysical Journal International 187, 613-630.

Ryder, I., Burgmann, R., Sun, J., 2010. Tandem afterslip on connected fault planes following the 2008 Nima-Gaize (Tibet) earthquake. J. Geophys. Res. 115, B03404.

Ryder, I., Parsons, B., Wright, T.J., Funning, G.J., 2007. Post-seismic motion following the 1997 Manyi (Tibet) earthquake: InSAR observations and modelling. Geophysical Journal International 169, 1009-1027.

Ryder, I., Wang, H., Bie, L., Rietbrock, A., 2014. Geodetic imaging of late postseismic lower crustal flow in Tibet. Earth and Planetary Science Letters 404, 136-143.

Savage, J., Prescott, W., 1978. Asthenosphere readjustment and the earthquake cycle. Journal of geophysical research 83, 3369-3376.

Shao, Z., Wang, R., Wu, Y., Zhang, L., 2011. Rapid afterslip and short-term viscoelastic relaxation following the 2008 Mw 7.9 Wenchuan earthquake. Earthquake Science 24, 163-175.

Shen, F., Royden, L., Burchfiel, B., 2001. Large-scale crustal deformation of the Tibetan Plateau. J. Geophys. Res 106, 6793-6816.

Shi, X., E. Kirby, H. Lu, R. Robinson, K. P. Furlong and E. Wang (2014). "Holocene slip rate along the Gyaring Co Fault, central Tibet." Geophysical Research Letters 41(16): 2014GL060782.

Tanner, W.F., 1995. Origin of beach ridges and swales. Marine Geology 129, 149-161.

Turcotte, D.L., Schubert, G., 2002. Geodynamics, 2nd ed. Cambridge University Press.

Unsworth, M.J., Jones, A.G., Wei, W., Marquis, G., Gokarn, S.G., Spratt, J.E., 2005. Crustal rheology of the Himalaya and Southern Tibet inferred from magnetotelluric data. Nature 438, 78-81.

Watts, A.B., 2001. Isostasy and Flexure of the Lithosphere. Cambridge University Press, Cambridge.

Watts, A.B., Burov, E.B., 2003. Lithospheric strength and its relationship to the elastic and seismogenic layer thickness. Earth and Planetary Science Letters 213, 113-131.

Wei, W., Unsworth, M., Jones, A., Booker, J., Tan, H., Nelson, D., Chen, L., Li, S., Solon, K., Bedrosian, P., 2001. Detection of widespread fluids in the Tibetan crust by magnetotelluric studies. Science 292, 716.

Wen, Y., Li, Z., Xu, C., Ryder, I., Bürgmann, R., 2012. Postseismic motion after the 2001 MW7.8 Kokoxili earthquake in Tibet observed by InSAR time series. Journal of geophysical research 117.

Willett, S.D., Chapman, D.S., Neugebauer, H.J., 1985. A thermo-mechanical model of continental lithosphere. Nature 314, 520-523.

Yamasaki, T., Houseman, G.A., 2012. The crustal viscosity gradient measured from post-seismic deformation: A case study of the 1997 Manyi (Tibet) earthquake. Earth and Planetary Science Letters 351–352, 105-114.

Zhang, C., Cao, J., Shi, Y., 2009. Studying the viscosity of lower crust of Qinghai-Tibet Plateau according to post-seismic deformation. Science in China Series D: Earth Sciences 52, 411-419.

Zhang, Z., Klemperer, S.L., 2005. West-east variation in crustal thickness in northern Lhasa block, central Tibet, from deep seismic sounding data. J. Geophys. Res. 110, B09403.

Zhao, W.-L., Morgan, W.J., 1987. Injection of Indian crust into Tibetan lower crust: A two-dimensional finite element model study. Tectonics 6, 489-504.

Zhao, W., Mechie, J., Brown, L.D., Guo, J., Haines, S., Hearn, T., Klemperer, S.L., Ma, Y.S., Meissner, R., Nelson, K.D., Ni, J.F., Pananont, P., Rapine, R., Ross, A., Saul, J., 2001.

Crustal structure of central Tibet as derived from project INDEPTH wide-angle seismic data. Geophysical Journal International 145, 486-498.

Figure captions

Fig. 1. Geological setting of the study area. Shown are two sesimic profiles around Siling Co. SF-2: Sino-French 2 (Zhang and Klemperer, 2005); INDEPTH-3 (International Deep Profiling of Tibet and the Himalaya) (Zhao et al., 2001). The map also shows the focal mechanisms (source: Global Centroid Moment Tensor Catalog, Ekström et al., 2012) of earthquakes occurred in this region that are discussed in the text. BNS: Bangong-Nujiang suture; TB: Tarim basin; QB: Qaidam basin; SB: Sichuan basin.

Fig. 2. Examples of geomorphic features characteristic of shorelines around Siling Co. (**A**) High resolution GeoEye satellite imagary showing the transition from depositional shorelines to wave-cut scarps along the highstand complex. Note the disected alluvial fans above the wave-cut scarp and the recessional beach ridges below; (**B**) Field photograph showing cuspate bar and back-bar developed along the highstand complex; (**C**) Low relief depositional surface atop the cuspate bar.

Fig. 3. (**A**) Localities of surveyed depostional highstand shorelines and OSL samples. The dark gray area represents the extent of the paleo-Lingtong highstand of Siling Co and the light blue area is the present lake extension. Color-coded circles denote three levels of confidence in the correlation of the shoreline with the Lingtong highstand level (see text and Supplemental Google Earth kmz file for detailed description). Sample numbers are labeled off the sample locations pointed by black arrows. **(B)** Variation in shoreline elevations along the radial distance away from the centroid of the water load (see location in Fig. 3A). **(C)** Variation in shoreline elevations along the radial distance away from the centroid of the water load that is projected onto the E-W line. Color-coded symbols in Fi.g 3B and Fig. 3C are the same as Fig. 3A.

Fig. 4. (**A**) Color-coded circles show the deviation (±2.3 m) of the shoreline elevations from their mean value of 4593.9 m. Other legends are the same as Fig. 3A. **(B)** reconstructred water load between the Lingtong highstand and the lake level in 1976 along profile ABC. (**C**) map view of the 3D geometry of the reconstructred water load.

Fig. 5. (**A-C**) Predicted crustal deflection pattern with T_e of 20, 30, and 40 km (from top to bottom) by forward elastic modeling. White lines are the contours of calculated deflection. Color-coded circles show the misfit between predicted deflections and observed deflections for confidence level A and B shorelines; the latter are represented by the deviation of the shoreline elevations from their mean value. (**D-F**) Comparison of shoreline elevation versus predicted deflections (T_e = 20, 30 and 40 km) at each surveyed highstand shoreline locality. Symbol legends are the same as Fig. 3.

Fig. 6. Black circles show the change in the maximum difference in calculated deflections (or deflection range) among shorelines of confidence levels A and B with T_e. Gray triangles show varying RMS of misfit between calculated and observed deflections with T_e. Both data sets show declining trends.

Fig. 7. Comparison of viscosities for different regions and variable timescales determined from post-seismic deformation after large earthquakes (labeled at bottom) and lacustrine shoreline deformation. Green and blue bars show viscosities determined from post-seismic and interseismic deformation, respectively. Red bars denote millennial timescale viscosities. Point-up or -down black arrows indicate viscosities with a lower or upper bound, respectively. The numbers represent the reference source of the viscosity estimates: 1. (Ryder et al., 2007); 2. (Yamasaki and Houseman, 2012); 3. (DeVries and Meade, 2013); 4. (Zhang et al., 2009); 5.

(Ryder et al., 2011); 6. (Wen et al., 2012); 7. (Hilley et al., 2009); 8. (Hilley et al., 2005); 9. (Shao et al., 2011); 10. (Huang et al., 2014); 11. (Ryder et al., 2010); 12. (Bie et al., 2014); 13. (Ryder et al., 2014); 14. (England et al., 2013).

Table 1. Field data and ages of OSL samples from the highstand shorelines around Siling Co.

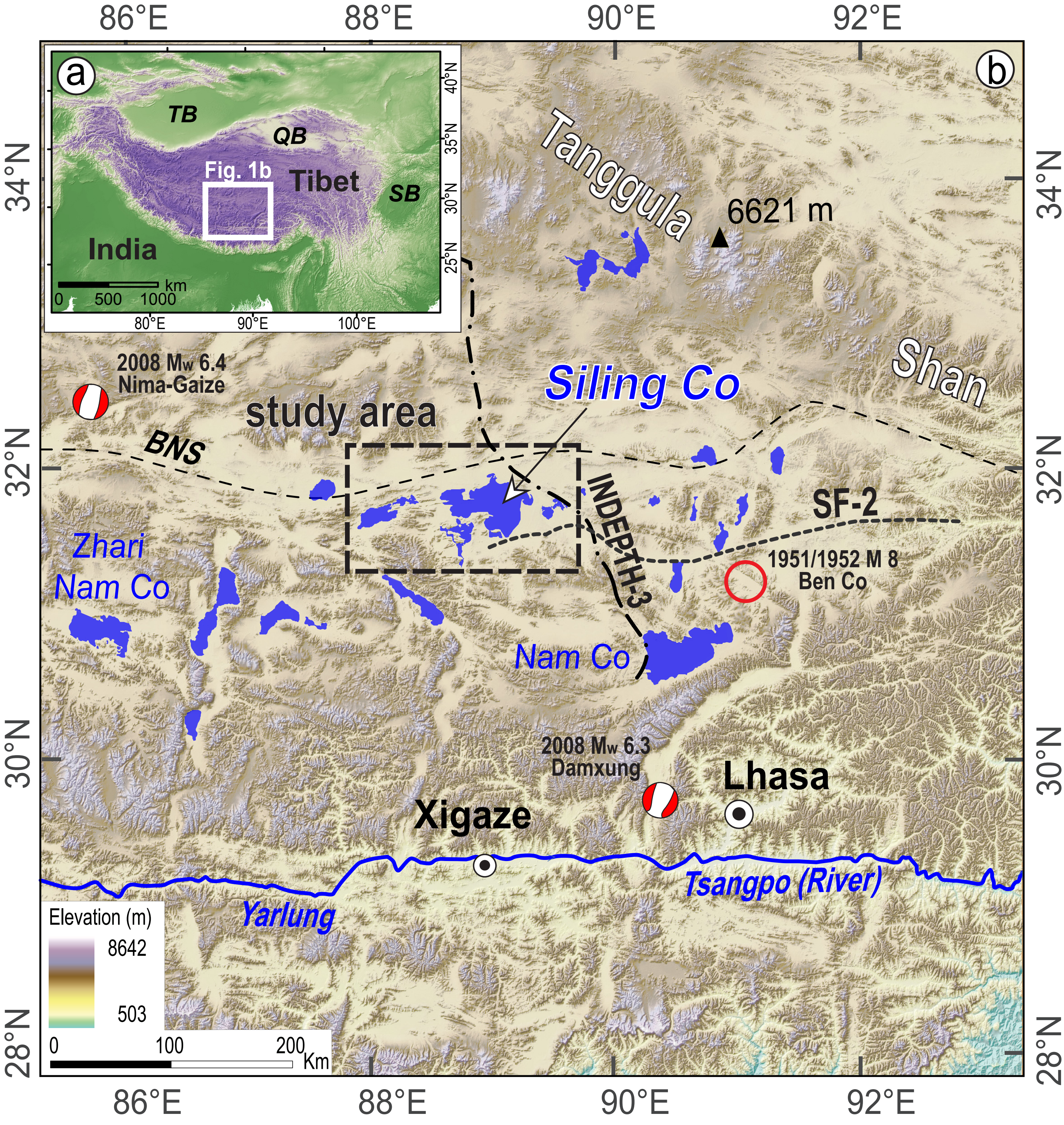

86°E
88°E
90°E
92°E
34°N
32°N
30°N
28°N
a
TB
QB
Tibet
SB
Fig. 1b
India
km
0 500 1000
80°E
90°E
100°E
25°N
30°N
35°N
40°N
b
Tanggula
6621 m
Shan
2008 Mw 6.4
Nima-Gaize
study area
Siling Co
BNS
INDEPTH-3
SF-2
Zhari
Nam Co
1951/1952 M 8
Ben Co
Nam Co
2008 Mw 6.3
Damxung
Lhasa
Xigaze
Yarlung
Tsangpo (River)
Elevation (m)
8642
503
0 100 200
Km

Fig. 1

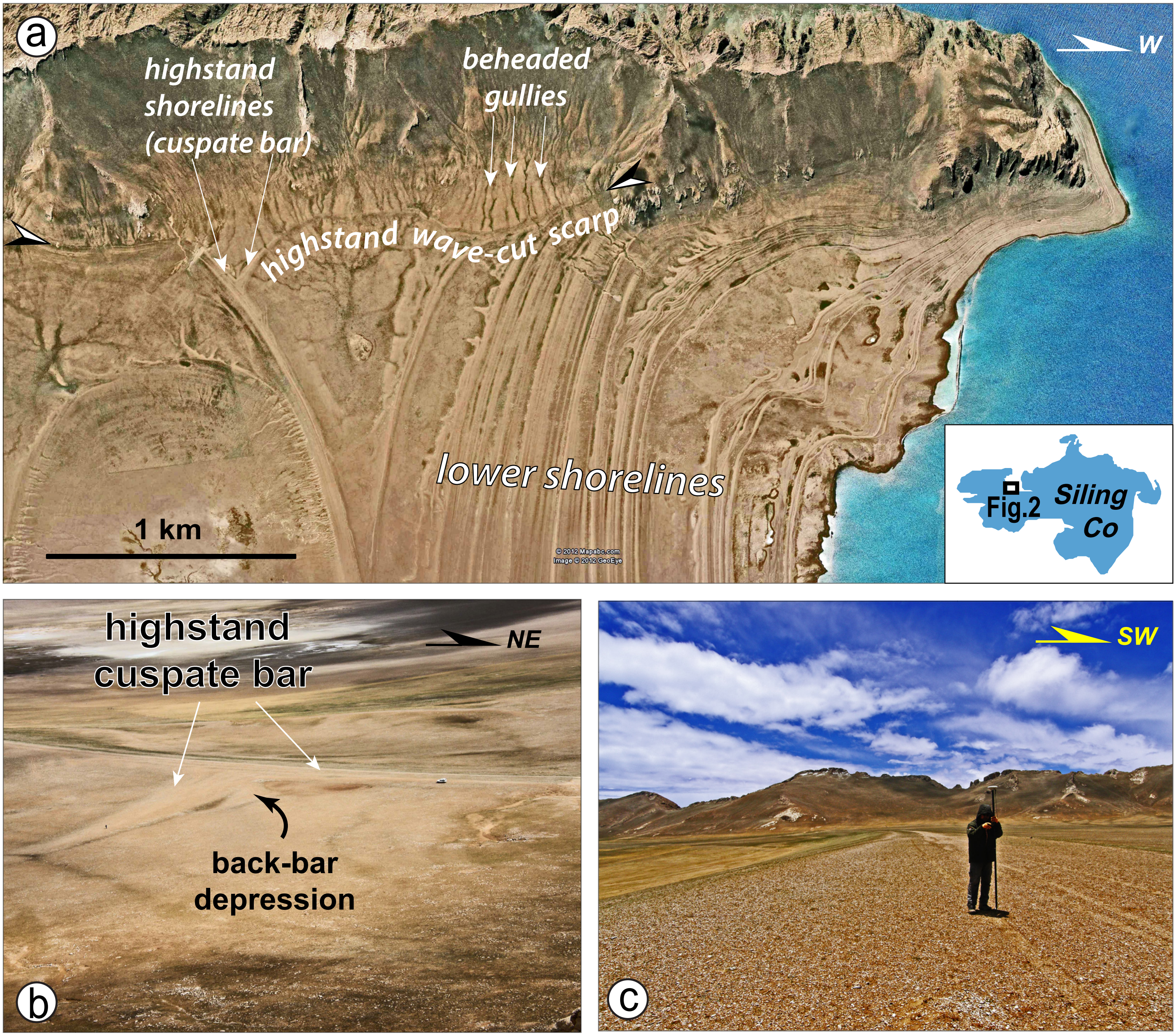
a
W
highstand
shorelines
(cuspate bar)
beheaded
gullies
highstand wave-cut scarp
lower shorelines
1 km
Fig.2
Siling
Co
b
highstand
cuspate bar
NE
back-bar
depression
c
SW

Fig. 2

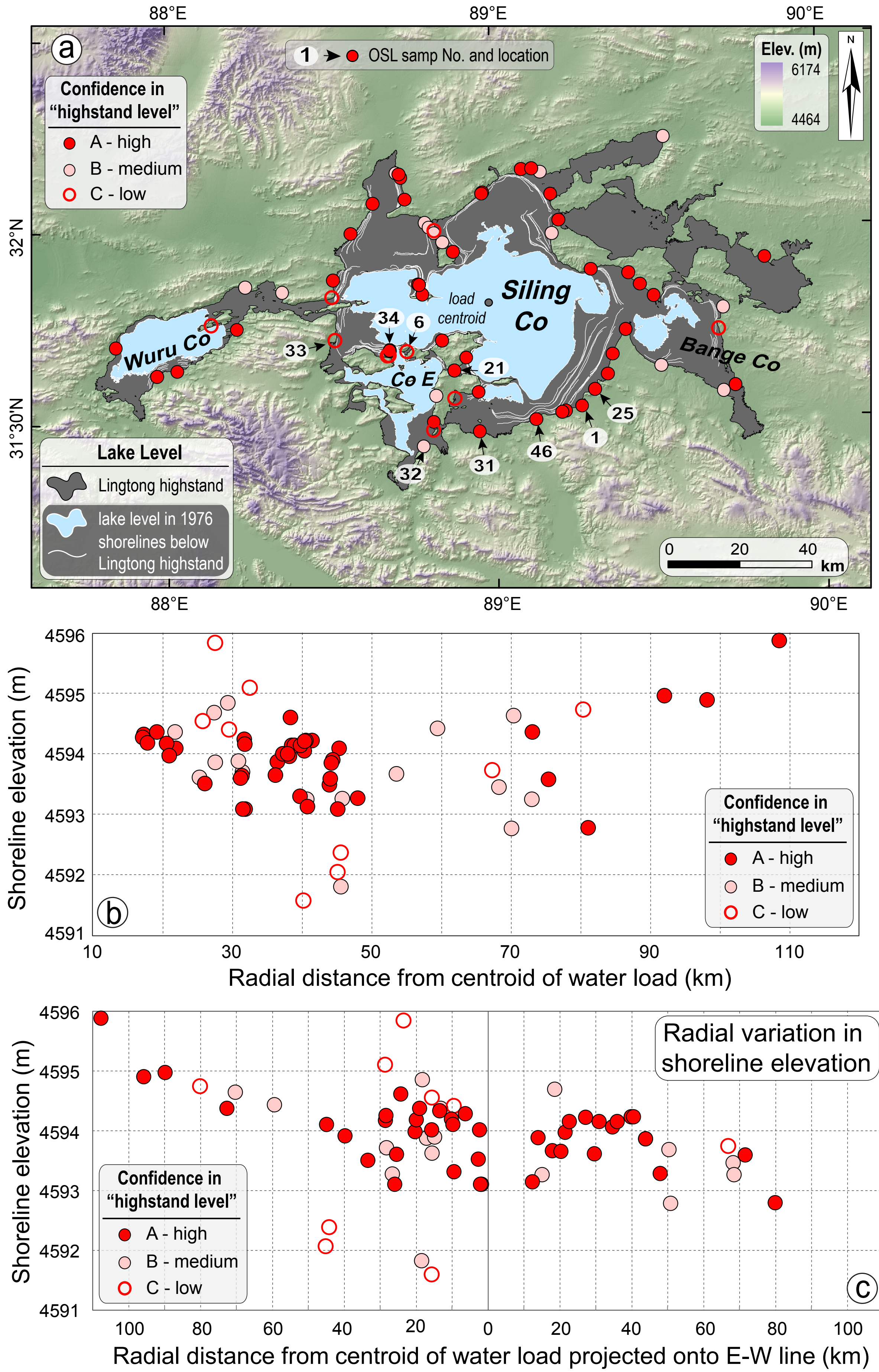
a
1 OSL samp No. and location
Confidence in "highstand level"
A - high
B - medium
C - low
Elev. (m)
6174
4464
N
Siling Co
load centroid
Wuru Co
Co E
Bange Co
34
6
33
21
25
1
46
31
32
Lake Level
Lingtong highstand
lake level in 1976
shorelines below Lingtong highstand
0 20 40 km
88°E
89°E
90°E
32°N
31°30'N
b
Shoreline elevation (m)
Radial distance from centroid of water load (km)
c
Radial variation in shoreline elevation
Radial distance from centroid of water load projected onto E-W line (km)

Fig. 3

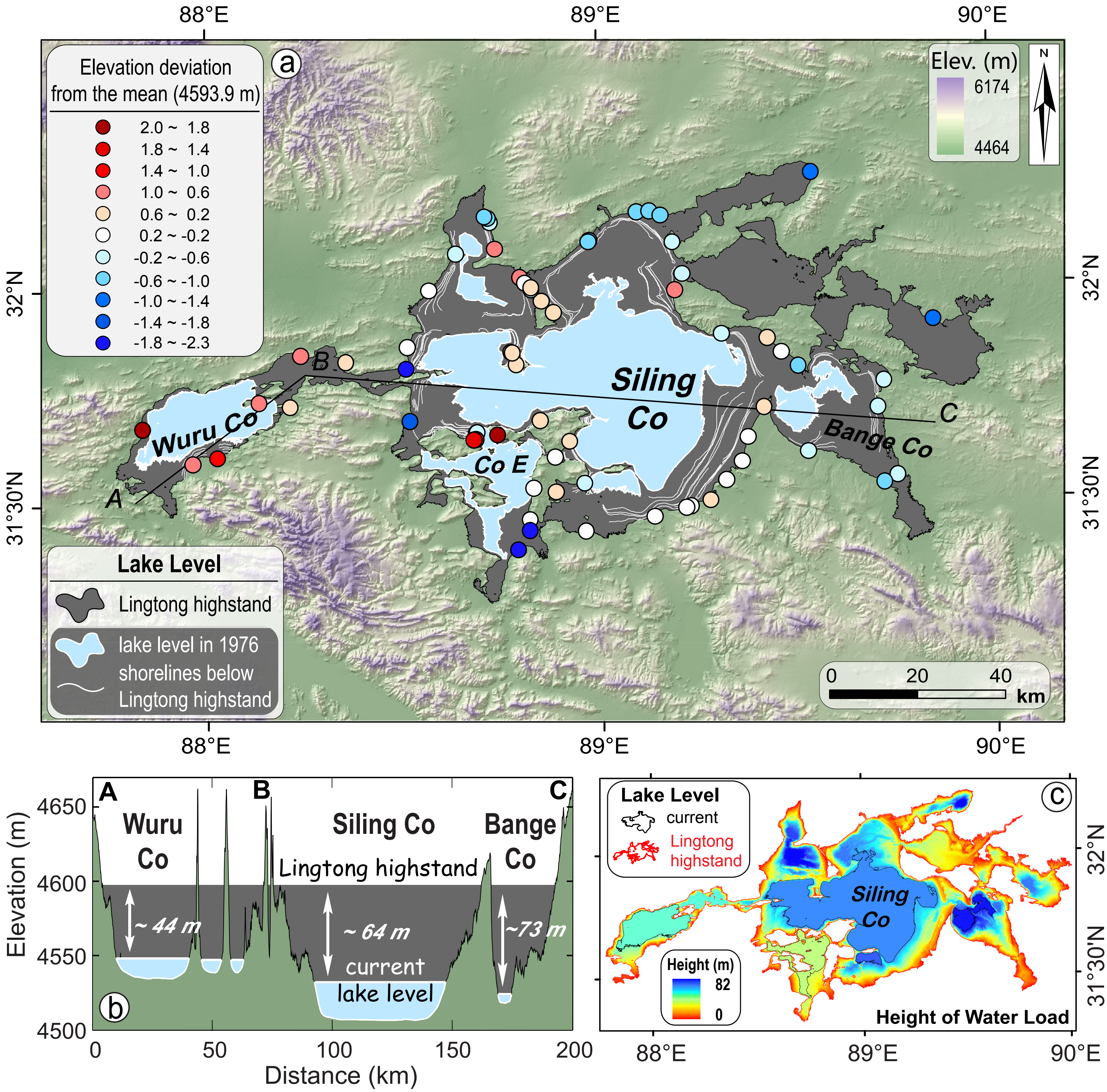
88°E
89°E
90°E
32°N
31°30'N
Elevation deviation from the mean (4593.9 m)
2.0 ~ 1.8
1.8 ~ 1.4
1.4 ~ 1.0
1.0 ~ 0.6
0.6 ~ 0.2
0.2 ~ -0.2
-0.2 ~ -0.6
-0.6 ~ -1.0
-1.0 ~ -1.4
-1.4 ~ -1.8
-1.8 ~ -2.3
a
Elev. (m)
6174
4464
N
Wuru Co
Siling Co
Co E
Bange Co
A
B
C
Lake Level
Lingtong highstand
lake level in 1976
shorelines below Lingtong highstand
0 20 40 km
Elevation (m)
4650
4600
4550
4500
Wuru Co
Siling Co
Bange Co
Lingtong highstand
~ 44 m
~ 64 m
~73 m
current lake level
b
0 50 100 150 200
Distance (km)
Lake Level
current
Lingtong highstand
Height (m)
82
0
Height of Water Load
c

Fig. 4

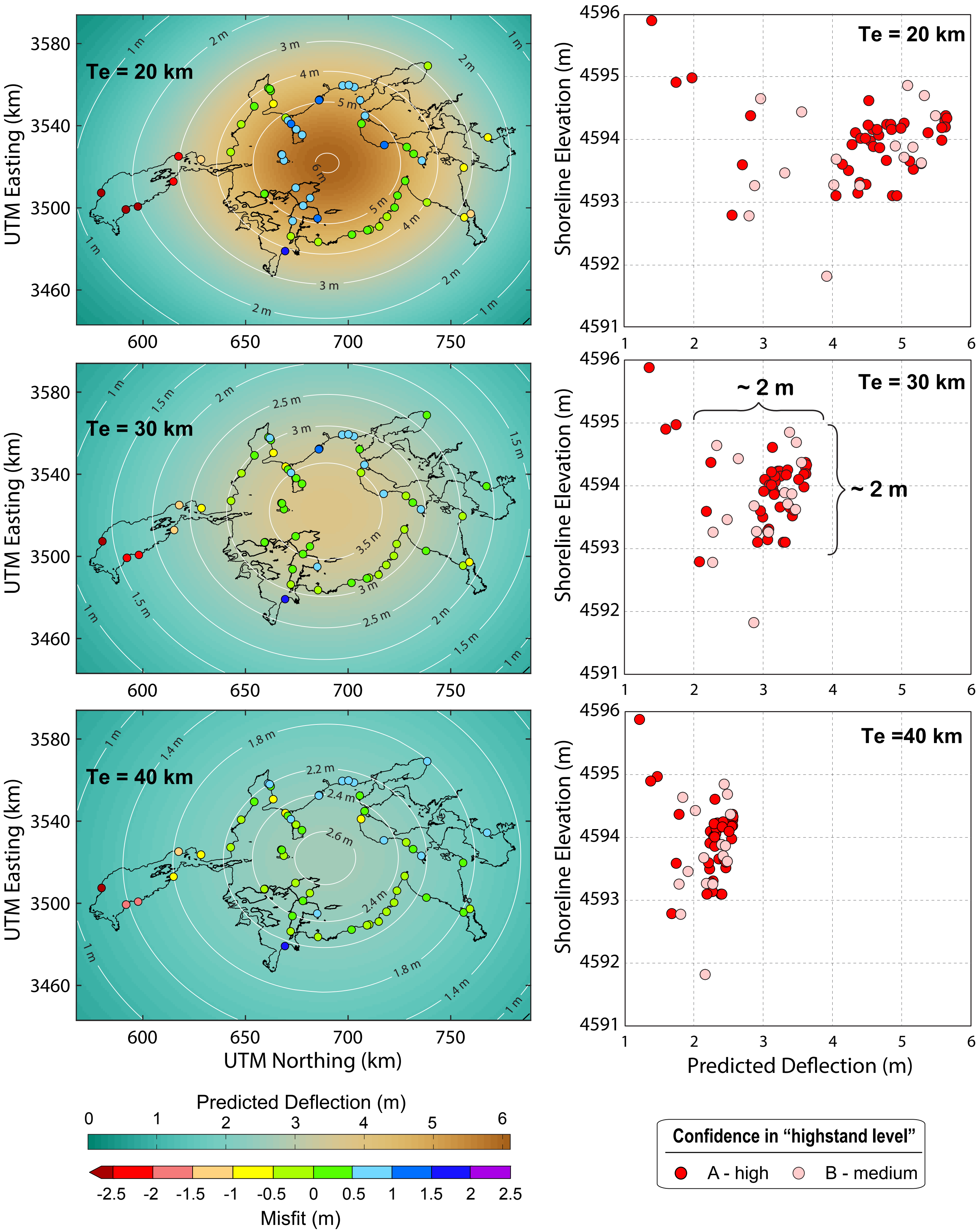

Te = 20 km
Te = 30 km
Te = 40 km
UTM Easting (km)
UTM Northing (km)
Shoreline Elevation (m)
Predicted Deflection (m)
~ 2 m
~ 2 m
Misfit (m)
Confidence in "highstand level"
A - high
B - medium

Fig.5

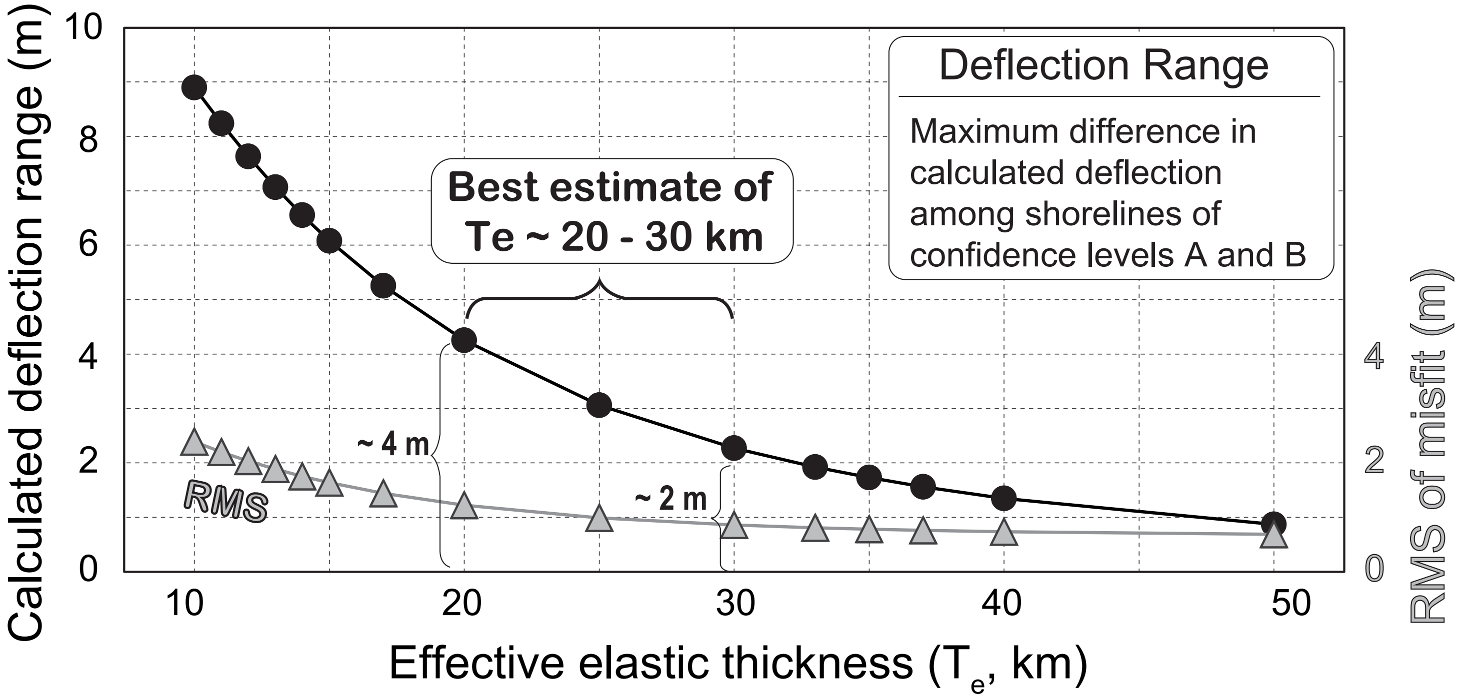
Calculated deflection range (m)
RMS of misfit (m)
Effective elastic thickness (Te, km)
Deflection Range
Maximum difference in calculated deflection among shorelines of confidence levels A and B
Best estimate of Te ~ 20 - 30 km
~ 4 m
~ 2 m
RMS
0
2
4
6
8
10
10
20
30
40
50

Fig. 6

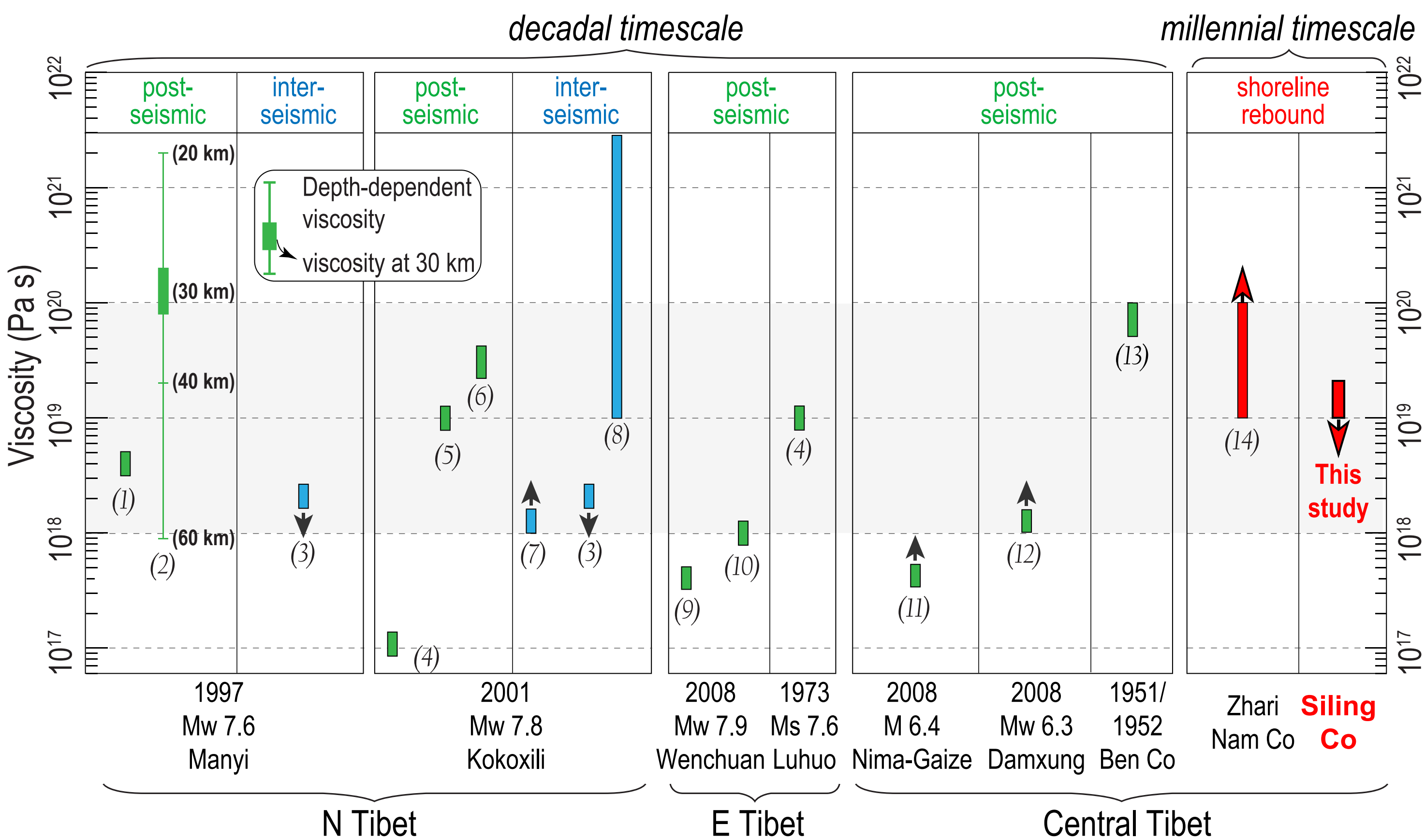

decadal timescale
millennial timescale
post-
seismic
inter-
seismic
post-
seismic
inter-
seismic
post-
seismic
post-
seismic
shoreline
rebound
Viscosity (Pa s)
10^{22}
10^{21}
10^{20}
10^{19}
10^{18}
10^{17}
(20 km)
(30 km)
(40 km)
(60 km)
Depth-dependent
viscosity
viscosity at 30 km
(1)
(2)
(3)
(4)
(5)
(6)
(7)
(3)
(8)
(9)
(10)
(4)
(11)
(12)
(13)
(14)
This
study
1997
Mw 7.6
Manyi
2001
Mw 7.8
Kokoxili
2008
Mw 7.9
Wenchuan
1973
Ms 7.6
Luhuo
2008
M 6.4
Nima-Gaize
2008
Mw 6.3
Damxung
1951/
1952
Ben Co
Zhari
Nam Co
Siling
Co
N Tibet
E Tibet
Central Tibet

Fig. 7

Table 1. Field data and ages of OSL samples from the highstand shorelines around Siling Co

Sample Name	Lat (°N)	Long (°E)	Elev (m)	Depth (m)	N (aliquots)	De (Gy)	Error (Gy)	Dose Rate (Gy/ka)	Error (Gy/ka)	Age (ka)	Error (ka)	Age Model*
XS-SL-OSL-O1A	31.524	89.216	4594	2.2	52	14.98	0.90	2.37	0.09	6.3	0.5	MAM-3
XS-SL-OSL-O1B	31.524	89.216	4594	2.2	52	12.05	0.67	2.37	0.09	5.1	0.3	MAM-3
XS-SL-OSL-O6	31.712	88.840	4594	2.3	53	6.92	0.50	1.74	0.07	4.0	0.3	MAM-3
XS-SL-OSL-O21A	31.633	88.877	4594	1.7	55	24.94	0.97	3.20	0.13	7.8	0.4	FMM
XS-SL-OSL-O21B	31.633	88.877	4594	1.7	55	12.58	0.88	3.20	0.13	3.9	0.3	FMM
XS-SL-OSL-O25	31.617	89.345	4594	1.3	56	10.74	0.68	2.48	0.10	4.3	0.3	MAM-3
XS-SL-OSL-O31	31.474	88.952	4594	0.5	56	15.51	1.09	3.04	0.07	5.1	0.4	MAM-3
XS-SL-OSL-O32	31.436	88.782	4592	1.7	53	4.25	0.31	2.74	0.05	1.5	0.1	MAM-3
XS-SL-OSL-O33	31.714	88.516	4592	1.7	51	15.62	0.92	2.98	0.06	5.2	0.3	MAM-3
XS-SL-OSL-O34	31.687	88.680	4594	0.4	56	11.91	0.63	2.60	0.06	4.6	0.3	MAM-3
XS-SL-OSL-O46	31.502	89.124	4594	1.4	52	14.98	0.90	2.37	0.09	6.3	0.5	MAM-3

* FMM – Finite mixture model; MAM – Minimum age model; numbers denote the component of each age model